Single Molecule Magnet Properties of Transition Metal Ions encapsulated in Lacunary Polyoxometalates: a Theoretical Study

Daniel Aravena,[a,*] Diego Venegas-Yazigi,[a,b] Eliseo Ruiz[c]

[a] Departamento de Química de los Materiales, Facultad de Química y Biología, Universidad de Santiago de Chile (USACH), Casilla 40, Correo 33, Santiago, Chile
[b] Centro Para El Desarrollo de Nanociencias y Nanotecnología, CEDENNA, Santiago, Chile
[c] Departament de Química Inorgànica and Institut de Química Teòrica i Computacional, Universitat de Barcelona, Diagonal 645, 08028 Barcelona, Spain

e-mail: daniel.aravena.p@usach.cl

Abstract

Single molecule magnet (SMM) properties of transition metal complexes coordinated to lacunary polyoxometalates (POM) are studied by means of state of the art *ab initio* methodology. Three $[M(\gamma\text{-}SiW_{10}O_{36})_2]$ ($M = Mn^{III}$, Fe^{III}, Co^{II}) complexes synthesized by Sato *et al.* (*Chem. Commun.* **2015**, *51*, 4081–4084) are analyzed in detail. SMM properties for the Co^{II} and Mn^{III} systems can be rationalized due to the presence of low energy excitations in the case of Co^{II}, which are much higher in energy in the case of Mn^{III}. The magnetic behavior of both cases is consistent with simple d-orbital splitting considerations. The case of the Fe^{III} complex is special, as it presents a sizable demagnetization barrier for a high spin d^5 configuration, which should be magnetically isotropic. We conclude that a plausible explanation for this behavior is related with the presence of low lying quartet and doublet states from the iron(III) center. This scenario is supported by *ab initio* Ligand Field analysis based on CASSCF results, that pictures a d-orbital splitting that resembles more a square-planar geometry than an octahedron, stabilizing lower multiplicity states. This coordination environment is sustained by the rigidity of the POM ligand, that imposes a longer axial bond distance to the inner oxygen atom in comparison to the more external, equatorial donor atoms.

1. Introduction

Since the discovery of slow relaxation of the magnetization properties in mononuclear Tb(III)-phthalocyanine compounds by Ishikawa *et al.*,[1] the quest of new Single Molecule Magnets (SMMs) with larger demagnetization barriers shifted from the synthesis of large polymetallic complexes with the highest possible multiplicity values toward lower nuclearity compounds. The rationale for the design of large, polymetallic compounds to achieve better SMMs was the maximization of the total spin of the system to achieve higher values for the demagnetization barrier. The relaxation barrier (U) is directly proportional to the squared spin value for the ground state ($U = DS^2$), where S is the total spin of the ground state and D is the zero field splitting parameter, which quantifies the energy splitting of the lowest energy multiplet, associated with magnetic anisotropy. In this way, larger spins would be more likely to yield higher values of U. Since 1995, when an Fe_{19} complex with S=33/2 was presented,[2] the record for the largest spin value of a single molecule was broken several times by different complexes, as Mn_9M_6 (M = Mo, W) (year 2000, S = 39/2),[3] Mn_{25} (year 2004, S = 51/2)[4] and Mn_{19} (year 2006, S = 83/2).[5] The current record value was presented in 2015 and corresponds to a Fe_{42} compound with S=90/2, in which 18 Fe^{III} centers are ferromagnetically coupled and the remaining 24 iron cations are low spin iron(II).[6]

Despite the success in the synthesis of molecules of increasingly higher spin, these systems did not present larger demagnetization barriers than existing, lower nuclearity compounds.[7–9] Furthermore, larger spin systems did not present any SMM properties in most cases. This apparent departure from the $U = DS^2$ relation can be understood noticing that the value of the zero field splitting parameter (D) is itself proportional to $1/S^2$, cancelling the explicit S^2 dependence of U.[10–12] Thus, chemical tuning of the coordination environment for the maximization of D is unavoidable to design improved SMMs, independently of their number of magnetic centers and total spin. Under this perspective, it is certainly simpler to conceive a tailored coordination environment for a single metal center in a small coordination compound than in a polynuclear compound, where the magnetic anisotropy of several centers has to be aligned and maximized simultaneously.

In this way, great attention is devoted to design new SMMs candidates using monometallic coordination compounds, where the environment for the metal center is carefully chosen to

maximize magnetic anisotropy.[13–16] The employment of rigid or bulky ligands to force a particular coordination environment by geometrical constraints or steric hindrance has proven to be a successful strategy to design new SMMs with improved properties. Apart for new lanthanide phthalocyanine complexes synthesized after $[TbPc_2]^-$,[17,18] we can mention several examples of remarkable SMMs based on polydentate, rigid or bulky ligands, as Dy^{III} sandwich complexes,[19] dicoordinate Fe^{I} and Ni^{I} compounds stabilized by bulky ligands[20,21] or endohedral lanthanide systems.[22] In this sense, lacunary polyoxometalates appear as promising ligands for SMM systems, given they large volume and extreme rigidity, that permits to design highly structured coordination environments for the promotion of magnetic anisotropy. Several examples of SMMs based on lanthanide magnetic centers coordinated to diamagnetic polyoxometalates exist in the literature, exhibiting large demagnetization barriers.[23,24] The influence of the polyoxometalate ligands in the energy splitting and magnetic anisotropy of the lanthanide ion has been studied in detail and has been rationalized and linked to Crystal Field Theory considerations.[25,26] In contrast, examples of polyxometalate-coordinated transition metal systems are comparatively scarce, and the relation between the observed SMMs properties and their electronic structure has not been yet described in detail.

The goal of this article is to analyze the SMMs properties of transition metal based complexes with polyoxometalate ligands by means of state of the art *ab initio* calculations. Sato *et al.*[27] reported magnetic studies about three transition metal complexes coordinated to two lacunary $[\gamma\text{-}SiW_{10}O_{36}]^{8-}$ silicontungstates, acting as tridentate ligands. Two of the studied compounds are field-induced SMMs, with demagnetization barriers of 6.3 cm^{-1} (Fe^{III}) and 13.4 cm^{-1} (Co^{II}) under a static field of 0.1 T. The third compound is based on Mn^{III} and shows temperature and frequency dependence for the ac magnetic susceptibility at very low temperatures, not allowing for the estimation of a demagnetization barrier. The coordination geometry around the transition metal centers is similar for the three complexes and can be described as distorted octahedral. Interestingly, the Fe based complex is assigned to be high spin Fe^{III}, with a formally isotropic d^5 configuration, being the only reported example of a high-spin d^5 system presenting SMM behavior. The article is divided in two parts: (i) the three studied systems are analyzed in terms of *ab initio* electronic structure calculations to describe the origin of their observed magnetic properties in terms of excitation energies, zero-field splitting, g-factors and *ab initio* Ligand Field analysis. (ii)

The case of high spin Fe^{III} presenting slow relaxation of the magnetization is studied in detail by *ab initio* methodologies. Computational results are analyzed to describe plausible and unlikely mechanisms for the unusual SMM properties reported for this compound.

2. Computational Details

All electronic structure calculations were performed using the ORCA 3.0.3 package.[28,29] Multireference *ab initio* calculations based on the Complete Active Space Self-Consisted field (CASSCF)[30,31] method considered the five orbitals of the 3d shell and dynamic correlation was included through the N-electron Valence State Perturbation Theory (NEVPT2).[32,33] Scalar relativistic effects were accounted by the Douglas-Kroll-Hess Hamiltonian at 2nd order (DKH2),[34–37] while state mixing due to spin orbit coupling was represented by a quasi-degenerate perturbation theory approach (QDPT). The effect of dynamic correlation was included in the QDPT step as a diagonal correction on the non-relativistic state energies. Molecular geometries for all complexes were directly obtained from X-Ray crystallographic structures.[27] As *ab initio* calculations are computationally demanding, truncated models of the three compounds were constructed keeping the immediate coordination environment of the transition metal ion and its second and third neighbors. Fourth neighbors were replaced with hydrogen atoms that were optimized to adjust their bond length, freezing the corresponding bond angles. In this way, the immediate coordination environment of the transition metal and its second neighbor W and Si atoms is preserved without any changes (See Figure 2). Cartesian coordinates for the molecular models are presented as Supporting Information. All calculations were performed using the DKH optimized SARC basis set for W,[38] and relativistically recontracted versions of the corresponding Ahlrichs basis set for the remaining atoms.[39,40] The COSMO solvation model with water as solvent was included in all calculations.[41] A comparison to gas-phase calculations for Fe^{III}-POM is presented in Table S2. d-orbital energies, spin orbit coupling and ligand field Hamiltonian parameters were directly fitted from CASSCF matrix elements by means of the *ab initio* Ligand Field (AILF) methodology.[42–44] In a nutshell, the AILF approach consists in the direct mapping of each matrix element of the configuration interaction matrix from a CASSCF calculation to a model Hamiltonian matrix. Dynamical correlation can be included by replacing the CASSCF excitation energies with corrected values (i.e. energies from a NEVPT2 run). In this case, the model Hamiltonian matrix was constructed in terms of usual Ligand Field Hamiltonian parameters (i.e. Racah parameters and

the general form of the ligand field matrix for d orbitals considering 15 parameters, which can be further condensed in terms of common ligand field approaches, such as Angular Overlap Model parameters).[45,46] In this way, the AILF approach treats high- and low-symmetry systems in an equal footing and can fit a larger set of parameters than a direct fit to state energies, as in considers all matrix elements of the configuration interaction matrix and not only its eigenvalues. NEVPT2 energies can eventually replace CASSCF values in the reconstruction of the *ab inito* CI matrix, while wavefunctions still correspond to a CASSCF calculation. Continuous shape measurements (CShM) were performed using the SHAPE 2.0 code.[47,48] CShM allows for a quantitative evaluation of the similarity between an arbitrary shape and reference shapes, discarding any effect associated with rotations and scaling. In practice, the degree of matching between target and reference shapes is expressed in terms of a number, where 0 indicates a perfect match that deteriorates with increasing values. As the studied compounds were six-coordinated, we compared the directly bonded MO_6 (M = Mn, Fe, Co) fragments with the octahedron, pentagonal pyramid and trigonal prism reference shapes.

3. Results and Discussion

According to a continuous shape measurement (CShM) analysis, the coordination environment of the three complexes can be described as close to octahedral, with S values of 1.88, 1.10 and 1.63 for Mn^{III}-POM, Fe^{III}-POM and Co^{II}-POM, respectively. All complexes can be described as axially elongated, where the longer bonds are associated with oxygen atoms of the SiO_4 fragment in the center of each lacunary polyoxotungstate. Equatorial oxygens are more external and belong to terminal W-O bonds. In terms of angles, the most notable distortion occurs in the O_{ax}-M-O_{eq} angles, which markedly depart from right angles to a maximum of 77°/103° in the case of Co^{II}-POM. This distortion is clearly produced by the tension associated with the M-O_{ax}-W-O_{eq} ring, where the differences in W-O and M-O bond lengths induce an opening of the M-O_{eq}-W angle. The orbital splitting of all complexes is expected to be close to the classical picture of octahedral geometry, with a sizable distortion due to the longer axial distances and angular deviation. Following the rules proposed by Gómez-Coca *et al.*[49] for the prediction of SMM behavior in transition metal complexes (see Figure 1), we can expect that the Mn^{III}-POM complex would hardly present a sizable relaxation barrier, given the large Jahn-Teller like distortion of their e_g orbitals and the absence of components of the angular momentum operator connecting the d_{x2-y2}

and d_{z2} orbitals, in line with its experimental behavior. The case of Fe^{III}-POM is interesting, as their high spin d^5 configuration would not be compatible with SMM behavior, conflicting with experimental results, this example will be analyzed in detail later. Finally, Co^{II}-POM is likely to present a relaxation barrier due to the excitations associated to the doubly and singly occupied t_{2g} orbitals. These orbitals are less affected by their coordination environment than e_g orbitals and are connected by matrix elements of the angular momentum operator. This orbital set is then suitable to develop a sizable demagnetization barrier, in agreement with their ac-susceptibility measurements.

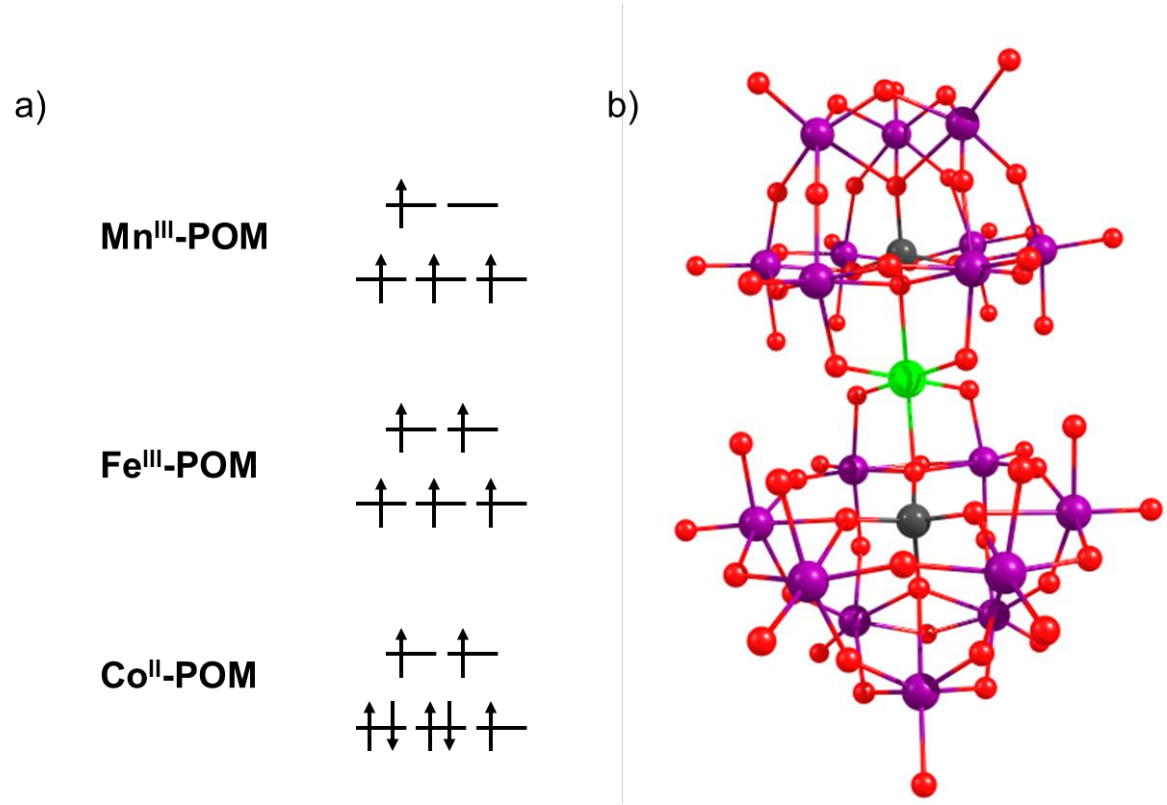

Figure 1. a) qualitative d-orbital diagrams for Mn^{III}-POM (top), Fe^{III}-POM (center) and Co^{II}-POM (bottom) assuming octahedral symmetry. b) Molecular structure of the studied complexes. Color code: M (Mn, Fe, Co), green; W, purple; Si, dark gray; O, red.

3.1 *ab initio* calculations: In order to describe the magnetic anisotropy of the ground state of the three studied complexes, we performed *ab initio* multiconfigurational calculations (CASSCF) for the model complexes, followed by a quasi-degenerate perturbation theory (QDPT) step to account for state interaction due to Spin-Orbit coupling (SOC). The CASSCF+QDPT method is widely

employed in the description of SMM complexes[15,43,50–52] because it allows for a multiconfigurational description of the ground and low energy excited states, which is a key condition to describe the state mixing due to SOC properly. In the QDPT step, nonrelativistic states from CASSCF are split in their corresponding M_s components that serve as the basis of the state interaction matrix associated with the SOC operator. In this way, wavefunctions after QDPT reflect the magnetic anisotropy of the system in their structure and allow for the evaluation of Spin-Hamiltonian parameters directly from their interaction with a magnetic field, without requiring any fit to a macroscopic magnetic response.

Considering the five 3d orbitals as the active space, a CASSCF(4,5) calculation was performed for Mn^{III}-POM considering 5 quintets, 45 triplets and 49 singlets. The lower two d orbitals are dominated by d_{xz} and d_{yz} contributions, with a small energy separation of 289 cm^{-1}, the d_{xy} orbital has an energy of 4288 cm^{-1} to complete the t_{2g} set for an ideal octahedral geometry. The d_{z2} orbital is a bit higher in energy (6948 cm^{-1}), while the d_{x2-y2} is markedly higher (19903 cm^{-1}) (See Figure 2). Under this scenario, the high-spin d^4 configuration for the ground state will be $(d_{yz})^1(d_{xz})^1(d_{xy})^1(d_{z2})^1$ and the first excitation energy is as large as 13449 cm^{-1}, due to the large destabilization of the d_{x2-y2} orbital that effectively quenches state mixing associated with SOC. The inclusion of NEVPT2 does not change this picture, yielding a slightly higher excitation energy (14237 cm^{-1}). The calculated splitting of the ground multiplet is 13.1 cm^{-1} and 13.5 cm^{-1} for CASSCF and NEVPT2, respectively, with a slight separation of the $M_L = \pm 2$ states due to some rhombic contribution to D (E/D = 0.03 for both methods). The combination of a relatively low barrier, together with the existence of some rhombic component in the ZFS and the non-Kramers' nature of the Mn^{III} ion are in line with the observed lack of measurable relaxation barrier for Mn^{III}-POM. Spin Hamiltonian parameters for all calculated models are presented in Table 1.

The calculated Zero Field Splitting (ZFS) parameter D is -3.27 cm^{-1} and -3.37 cm^{-1} for CASSCF and NEVPT2, respectively. These values are lower than the experimentally fitted D value (-5.28 cm^{-1}), as reflected by the comparison of the experimental and calculated susceptibility curves (see Figure 3). In the low temperature range, the decrease of the χT product is more pronounced in the experimental curve, in line with the higher experimental value of D in comparison to calculations. The origin of this discrepancy relies in the importance of quintet-triplet excitations for a

quantitative recovery of magnetic anisotropy. An analysis of the contributions of each excited state to the value of D reveals that quintet-quintet excitations contribute only ~ -1.2 cm^{-1} to D, which is -3.19 cm^{-1} in the second order perturbation theory approach based on a CASSCF(4,5) calculation. It is remarkable that several quintet-triplet excitations contribute importantly to the zero field splitting value (see Table S1 for a complete list of contributions for all quintet, triplet and singlet states). It is important to stress that zero field splitting values originating from lower multiplicity states are expected to be underestimated in CASSCF calculations, are higher multiplicity states are over stabilized under this methodology, yielding too large energy differences with respect to lower multiplicity states. This issue will manifest more clearly in the case of Fe^{III}-POM, where magnetic anisotropy is essentially related to sextet-quartet excitations.

Table 1. Calculated Spin-Hamiltonian parameters for Mn^{III}-POM, Fe^{III}-POM and Co^{II}-POM for CASSCF(n,5) calculations. Presented zero-field splitting parameters (D) are based on second oreder perturbation theory (2PT) and effective Hamiltonian approaches (H_{eff}). g-factors for the lowest Kramer's doublets are tabulated for Co^{II}-POM and Fe^{III}-POM. ΔE_{sf} refers to the first three spin-free excitations.

		D (cm^{-1}), [E/D]		g-factors			ΔE_{sf} (cm^{-1})
		2PT	H_{eff}	g_x	g_y	g_z	
Co^{II}-POM	CASSCF(7,5)	-243.7 [0.12]	102.0 [0.28]	2.385	2.614	7.575	266.7
				1.177	2.778	4.416	726.1
							5101.3
Co^{II}-POM	NEVPT2	-119.4 [0.18]	80.6 [0.31]	2.025	2.621	7.516	511.6
				1.906	2.363	5.230	972.5
							6749.3
Fe^{III}-POM	CASSCF(5,5)	-0.33 [0.04]	-0.32 [0.05]	0.035	0.037	10.003	23566.5
				1.208	1.247	5.910	24543.8
				1.912	4.728	7.185	24674.1
Fe^{III}-POM	NEVPT2	-0.38 [0.07]	-0.37 [0.09]	0.091	0.101	9.986	17097.3
				1.987	2.083	5.732	17915.7
				1.749	3.826	7.906	18006.4
Mn^{III}-POM	CASSCF(4,5)	-3.19 [0.03]	-3.28 [0.03]				13449.6
							16418.9
							17511.0
Mn^{III}-POM	NEVPT2	-3.27 [0.03]	-3.37 [0.03]				14236.4
							14676.3
							15267.5

The case of Co^{II}-POM is different, as it presents relatively low-lying first and second excited states at 266.7 cm^{-1} and 726.1 cm^{-1}. These states cannot be described by a single d orbital filling, as they correspond to mixtures of various configurations, in which the $t_{2g}^5e_g^2$ type is predominant (assuming the labelling for octahedral symmetry). In terms of d-orbital energies, we observe that the first three orbitals are mixtures of d_{xy}, d_{xz}, and d_{yz} with energies 0 cm^{-1} (reference), 649 cm^{-1} and 1055 cm^{-1}. The most antibonding orbitals have energies of 6259 cm^{-1} (d_{z2}) and 7964 cm^{-1} (d_{x2-y2}). The calculated D parameter is 102.0 cm^{-1} and E/D is 0.28 and accounts for a splitting between the first and second Kramers' doublets of 226.5 cm^{-1}. These parameters yield a susceptibility curve that matches the experimental trend (see Figure 3) and agree with values fitted to experiment (D = 95.2 cm^{-1} and E/D = 0.075). Furthermore, the calculated g-factors for the first Kramers' doublet are strongly anisotropic ($g_z = 7.58$, $g_y = 2.61$ and $g_x = 2.39$), in agreement with the published values obtained from EPR measurements (6.76, 3.31 and 1.88).[27] The marked departure for perfectly axial anisotropy reflects in the orientation of the main anisotropy axis for the first Kramers' doublet (see Figure S1). In the cases of Fe^{III}-POM and Mn^{III}-POM, E/D values are small and the main anisotropy axis aligns with the z axis, while CoII-POM anisotropy is not aligned with the coordinae frame defined by the direction of the M-L bonds. The large value of E/D can be related with efficient relaxation by direct tunneling and is consistent with a relatively low value for the experimental Orbach barrier (13.4 cm^{-1}) and the requirement of a static magnetic field for the observation of SMM behavior.

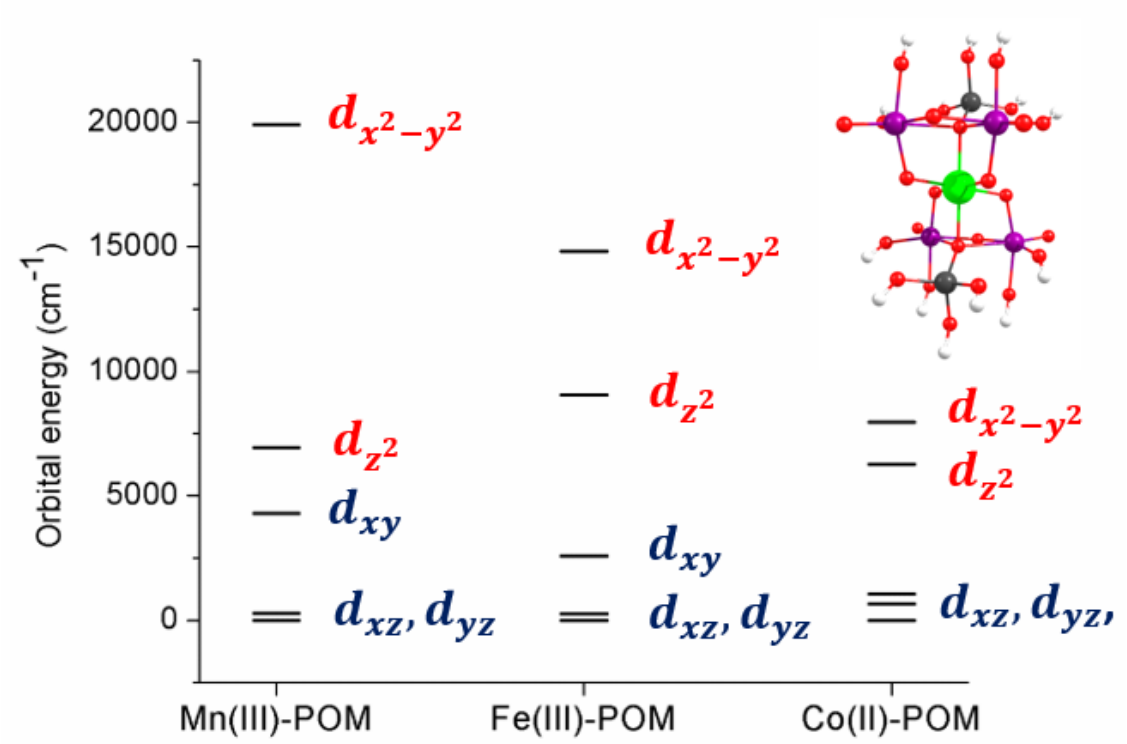

Figure 2. *ab initio* Ligand Field derived d-orbital diagrams for Mn^{III}-POM (left), Fe^{III}-POM (center) and Co^{II}-POM (right). In the all cases, the source calculation corresponds to a NEVPT2 corrected CASSCF(n,5) run with an active space composed by the five 3d orbitals and n = 4, 5 and 7 for Mn^{III}-POM, Fe^{III}-POM and Co^{II}-POM, respectively. (top, right) Simplified structure employed in the calculations, color code: M (Mn, Fe, Co), green; W, purple; Si, dark gray; O, red.

We now turn our attention to the case of Fe^{III}-POM, that appears to conflict with common conceptions in the field of transition-metal based SMMs. It presents a high-spin d^5 configuration, which is related with a ground sextet that is likely to mix weakly with excited states of lower multiplicities. Orbital energies corresponding to a NEVPT2 corrected, CASSCF(5,5) calculation including 1 sextet, 24 doublets and 75 singlets follow the same pattern of Mn^{III}-POM, as the first two orbitals are a mixture of the d_{xz} and d_{yz} orbitals, with an energy separation of 269 cm^{-1}. The d_{xy}, d_{z2} and d_{x2-y2} orbitals follow at 2594 cm^{-1}, 9038 cm^{-1} and 14825 cm^{-1}, respectively. Again, orbital energies resemble the ordering of a square-planar complex due to the longer Fe-O distance induced by the rigidity of the POM ligand. As expected, the ground state corresponds to a sextet state, separated by 23566 cm^{-1} from the lowest energy quartet. The inclusion of dynamical correlation by NEVPT2 diminishes the sextet-quartet gap to 17097 cm^{-1}. In both cases, the energy

separation is too high to allow for an efficient state mixing by Spin-Orbit coupling, resulting in too low D values (-0.32 cm^{-1} and -0.37 cm^{-1} for CASSCF and NEVPT2, respectively). The energy splitting for the ground sextet is around 2 cm^{-1} for both methods, too low to explain the SMM properties of the Fe^{III}-POM complex. Comparing the experimental and simulated magnetic susceptibility curves (see Figure 3), it is clear that the calculation is not completely capturing the magnetic anisotropy of the Fe^{III}-POM system, as the calculated decay of χT at low temperatures associated with magnetic anisotropy is too steep. This difference is reflected in the considerably higher value of the experimentally fitted zero field splitting parameter (D = -1.20 cm^{-1}).[27] As mentioned earlier, the origin of this discrepancy is the predominance of sextet-quartet excitations in magnetic anisotropy, associated with an underestimation of D.

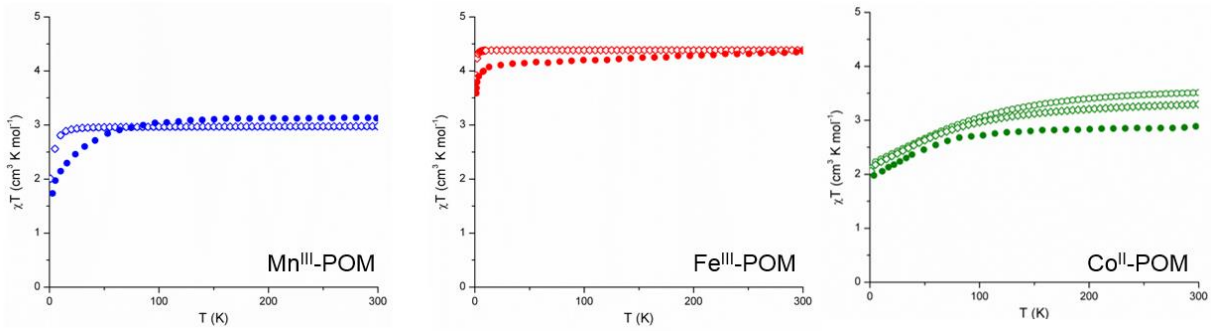

Figure 3. Experimental (filled circles), CASSCF (empty circles) and NEVPT2 (empty diamonds) magnetic susceptibility curves for Mn^{III}-POM (left, blue), Fe^{III}-POM (left, center) and Co^{II}-POM (right, green). In the case of Mn^{III}-POM and Fe^{III}-POM, CASSCF and NEVPT2 curves superimpose.

3.2 Extended active space calculations

To obtain a more accurate description of the electronic structure of the three studied complexes, we performed CASSCF(n+4,7) calculations for all models. We are especially interested in Fe^{III}-POM and Mn^{III}-POM, where a clear underestimation of the zero field splitting was observed in CASSCF(n,5) calculations. The extended active space now includes the bonding counterparts of the antibonding d_{z2} and d_{x2-y2} orbitals. As observed in Table 2, extended active space calculations do not differ significantly from CASSCF(n,5) results. The most interesting change occurs in Fe^{III}-POM, where the D value increases from -0.38 cm^{-1} to -0.51 cm^{-1} upon extension of the active space (NEVPT2 results). On the contrary, CASSCF values for both active spaces are similar (-0.33 cm^{-}

[1] and -0.38 cm^{-1} for 5 and 7 active orbitals, respectively). This contrasting behavior is connected to the calculated sextet-quartet gap in all cases, as the largest D value is associated with the lowest energy gap (D = -0.51 cm^{-1}, ΔE = 13566 cm^{-1}), while other calculations predict larger energy splittings (23566 cm^{-1}, 17097 cm^{-1} and 20920 cm^{-1} for the CASSCF(5,5) calculation, its corresponding NEVPT2 run and CASSCF(9,7), respectively). A quantitative estimation of spin state energetics should yield a better agreement between experimental and calculated zero field splitting parameters. Unfortunately, such task has proven to require even larger calculations and eventually explicit consideration of intermolecular interactions.[53,54] These requirements are beyond the scope of our model calculations.

Table 2. Selected Spin-Hamiltonian parameters for Mn^{III}-POM, Fe^{III}-POM and Co^{II}-POM for extended active space calculations. Presented zero-field splitting parameters (D) are based on second oreder perturbation theory (2PT) and effective Hamiltonian approaches (H_{eff}). g-factors for the lowest Kramer's doublets are tabulated for Co^{II}-POM and Fe^{III}-POM.

		D (cm^{-1}), [E/D]		g-factors			ΔE_{sf} (cm^{-1})
		2PT	H_{eff}	g_x	g_y	g_z	
Co^{II}-POM	CASSCF(11,7)	-236.2 [0.12]	101.6 [0.28]	2.383	2.635	7.566	273.8
				1.207	2.752	4.470	729.3
							5114.7
Co^{II}-POM	NEVPT2	-129.5 [0.18]	84.9 [0.29]	2.076	2.626	7.547	
				1.832	2.438	5.127	
Fe^{III}-POM	CASSCF(9,7)	-0.38 [0.05]	-0.36 [0.06]	0.043	0.046	10.000	20920.3
				1.408	1.463	5.874	21960.4
				1.879	4.501	7.374	22072.0
Fe^{III}-POM	NEVPT2	-0.51 [0.07]	-0.50 [0.09]	0.103	0.115	9.985	13566.2
				2.036	2.136	5.716	13917.3
				1.735	3.765	7.949	14053.2
Mn^{III}-POM	CASSCF(8,7)	-2.83 [0.03]	-2.90 [0.03]				14508.7
							17582.6
							17934.9
Mn^{III}-POM	NEVPT2	-2.93 [0.03]	-3.02 [0.03]				14664.9
							15140.0
							15555.9

3.3 The case of Fe^{III}-POM

If we consider the d-excitation energy manifold for a square-planar complex, a sizable magnetic anisotropy could be achieved if lower multiplicity states stabilize with respect to the ground sextet, yielding low energy excitations that can couple through the SOC operator. This is related with the strong destabilization of the d_{x2-y2} orbital, which is directly pointing towards the four equatorial ligands. In this way, S=3/2 electronic configuration will be not so disfavored by the enhanced repulsion due to electron pairing, as it will be partially compensated by the depopulation of the significantly antibonding d_{x2-y2} orbital. In the case of Fe^{III}-POM, it was already commented that CASSCF results predict the lowest quartet to be 23539 cm^{-1} higher in energy than the ground sextet. The inclusion of NEVPT2 results in a smaller energy gap of 17063 cm^{-1}, which is still too high to explain the observed relaxation barrier of Fe^{III}-POM. The calculated zero field splitting parameter modestly increased from CASSCF (-0.32 cm^{-1}) to NEVPT2 (-0.37 cm^{-1}).

A similar underestimation of D has been observed by Stavretis *et al.* for high spin Fe^{III} porphyrin complexes coordinated to halogens.[55] The authors relate this trend to the too ionic picture of CASSCF due to its lack of dynamical correlation effects, which is only partially corrected by NEVPT2. From a linear regression of calculated results with respect to experimental D values, the authors propose a scaling for the calculated D values (depending if they are derived from CASSCF or NEVPT2 calculations) to match accurate reference data obtained from INS measurements. If we apply the proposed scaling, the D parameters would be -1.67 cm^{-1} (CASSCF) and -4.49 cm^{-1} (NEVPT2), being in the right order of magnitude for the experimental D parameter (-1.20 cm^{-1}) for Fe^{III}-POM.[27] In our case, D values for CASSCF and NEVPT2 are similar, in contrast with results from Stavretis *et al.*,[55] where a three-fold increase in D is observed for NEVPT2 results. This difference is likely to be related with the larger covalency for the Fe^{III}-porphyrin complexes in comparison with Fe^{III}-POM. Opposed to the case of Co^{II}-POM, we expect a smaller decrease of the relaxation barrier associated to other relaxation mechanism in Fe^{III}-POM due to the lack of nuclear spin of the most stable isotope of iron, the negative sign of the zero field splitting parameter and its lower rhombic component. Coupling of electronic and nuclear spin has been pointed as the main factor governing magnetic relaxation in mononuclear Co compounds (I=7/2).[56]

To visualize the relation between interelectronic repulsion, the sextet-quartet gap and its relation with D, a correlation diagram for Fe^{III}-POM was constructed from *ab initio* ligand field parameters (see Figure 4, left). First, a CASSCF(5,5) calculation including 1 sextet, 24 quartets and 75 doublets was performed and NEVPT2 corrected energies were obtained from the former calculation. Then, Racah B and C ligand field parameters were fitted from the CI matrix reconstructed from NEVPT2 energies and CASSCF wavefunctions. As a check of the accuracy of the fitted parameters, state energies were simulated directly from a ligand field Hamiltonian, obtaining a satisfactory match with respect to source NEVPT2 energies (mean absolute deviation = 196.5 cm^{-1}, considering all roots of all multiplicities derived from d^5 configuration). Similar to a Tanabe-Sugano diagram,[57,58] we plotted the evolution of energy splitting for Fe^{III}-POM from the free ion (no ligand field) to the strong field limit as a function of the ratio between ligand field strength and interelectronic repulsion. This is analogous to the Δ_o/B ratio employed in the Tanabe-Sugano diagrams based on an octahedral coordination environment. To achieve the free ion limit, we obtained the state energies from a ligand field Hamiltonian setting all ligand field parameters to zero but maintaining the Racah B and C parameters fixed. From left to right in the x axis, we set an increasing multiplicative factor for the ligand field splitting and kept B and C fixed, obtaining an increasing "Δ_o/B" ratio. When the multiplicative factor is equal to 1, no scaling between ligand field and Racah parameters is performed and the source NEVPT2 energies are recovered. Values larger (smaller) than 1 in the x axis represent a larger (smaller) "Δ_o/B" ratio than the obtained in the *ab initio* calculations.

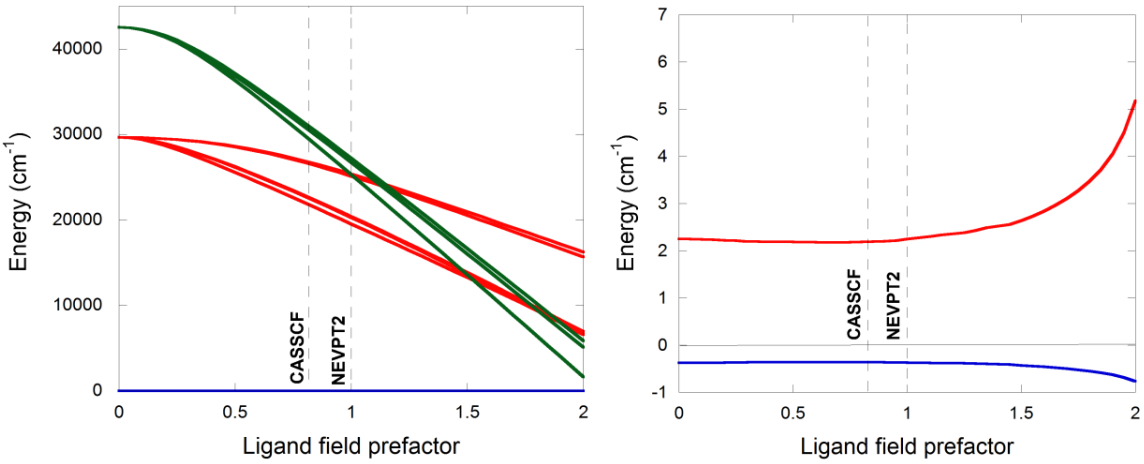

Figure 4. Left: correlation diagram for the energy splitting of d-d transitions constructed from the *ab initio* Ligand Field parameters for the Fe^{III}-POM complex (NEVPT2 calculation) with a Ligand field prefactor equivalent to the "Δ_o/B" ratio of Tanabe-Sugano diagrams. Sextets, quartets and doublets are represented in blue, red and green, respectively. For clarity, only the only sextet and the lowest five quartets and three doublets are printed. As NEVPT2 derived values are taken as reference, the splitting pattern for NEVPT2 correspond to a factor of 1.0 of the ligand field strength (unscaled). The value for CASSCF is 0.82, indicating that the ratio between ligand field splitting and interelectronic (Racah) repulsion is smaller than NEVPT2. Right: dependence of the D parameter (blue) and the multiplet splitting of the ground sextet (red) as a function of the ligand field to interelectronic repulsion parameter obtained from QDPT calculations.

Following the evolution of the energy gap between the ground sextet and its proximal excited states (Figure 4, left), it is clear that larger "Δ_o/B" ratio will be favorable for a lowering of this excitation energy. Furthermore, this induces a marked increase of the zero field splitting parameter when low energy excitation become proximal (Figure 4, right). In order to achieve a D value close to experiment (-1.2 cm^{-1}), the ratio between ligand field and interelectronic repulsion must be larger than the obtained for NEVPT2. To put this trend in context, we can estimate the position for CASSCF calculation in the correlation diagram, being lower than the NEVPT2 value (0.82, as marked with a vertical line in Figure 4, left). Equation 1 is an empirical way to estimate the decrease in B parameter (nephelauxetic reduction) due to metal-ligand orbital mixing. B_0 corresponds to the free ion value of B and h and k are empirical parameters for ligand and metal, respectively. h and k are fitted from spectroscopic data to account for the observed reduction of the Racah parameters for several complexes with different combinations of transition metals and ligands and are designed to be transferable.

$$\frac{B-B_0}{B_0} = h * k \quad (1)$$

Using equation 1, we estimate a B value around 700 cm^{-1} for Fe^{III}-POM, considering typical values for the nephelauxetic reduction parameters (0.24 for k_{FeIII} and 1.5 for h_L, if we assume ox^{2-} as representative of our ligand),[59] and a free ion B parameter for Fe^{III} of 1139 cm^{-1}, calculated from a fit of all sextet-quartet excitations.[60] This estimated value is significantly lower than the NEVPT2

result for B (987 cm^{-1}), indicating that a larger correction is required to achieve a lower Racah parameter and a higher D. In this way, it appears that NEVPT2 is correcting in the right direction, although insufficiently, from the crude overestimation of Racah parameters inherent of the CASSCF method. As discussed previously, this picture is consistent with results from Stavretis *et al.* for iron(III) porphyrins.[55] The behavior of CASSCF is expected due to the neglect of dynamical correlation of this method. In this way, the repulsion between electrons is overestimated and excitation energies tend to be higher than experiment. Furthermore, covalency is likely to be underestimated for the same reasons, resulting in a too low "Δ_o/B" ratio. In its current form, NEVPT2 only corrects state energies, without affecting CASSCF wavefunctions, inheriting its deficiencies. Concretely, it is expected that CASSCF wavefunctions with larger active spaces (for instance, including bonding-antibonding pairs) will yield a better description of metal-ligand covalency, improving both CASSCF and NEVPT2 results but increasing the computational cost of the calculations. Under this picture, it is expected that CASSCF and NEVPT2 methods will yield lower zero field splitting parameters than experiment if electronic excitations that contribute to D belong to different terms. This situation is normally not encountered in compounds with higher anisotropy (for instance, in Co^{II}-POM), where low energy excitation belongs to states stemming from the same multiplet.

4. Conclusions

The combination of *ab initio* calculations and *ab initio* Ligand Field analysis allowed for the identification of the key features responsible for the magnetization relaxation properties of the three studied complexes. In the case of Co^{II}-POM, SMM properties are related with the presence of a strong unquenched angular momentum in the ground state, associated to low lying d excitations. The calculated zero field splitting parameter is larger than the experimental value, in agreement with the contribution of additional relaxation mechanisms, such as the interaction with the nuclear spin (I=7/2) of the cobalt center. In the case of Mn^{III}-POM, its lack of a measurable relaxation barrier is consistent with the absence of low lying excited states for this complex, with a relatively low zero field splitting parameter that is reasonably reproduced by *ab initio* methods. Fe^{III}-POM is the most challenging case, as it exhibits a measurable, although small, relaxation barrier for a formally isotropic d^5 configuration. *ab initio* results point to the axially elongated coordination environment forced by the rigidity of the lacunary POM ligand as the main factor for

the unusual SMM properties of Fe^{III}-POM. In this way, the orbital splitting pattern of the studied compounds is best described as close to square-planar instead of near octahedral. The strong destabilization of the d_{x2-y2} orbital results in a lowering of the sextet to quartet gap, allowing for a moderate spin mixing and the development of some magnetic anisotropy. The presented *ab initio* calculations underestimate the zero field splitting due to the too repulsive picture of CASSCF associated with missing dynamical correlation. NEVPT2 only partially corrects this deficiency, reflected in an overestimation of the interelectronic repulsion parameters, thus giving a lower nephelauxetic reduction. A reasonable estimation of the nephelauxetic reduction yields an energy splitting that is compatible with the presence of a small demagnetization barrier, in line with the experimentally measured value. In this way, lacunary polyoxometalates are excellent candidates for the design of highly structured and rigid coordination environments for transition metal based SMMs, favoring the development of sizable magnetic anisotropy. Concretely, POM ligands can force a specific coordination environment, overcoming coordination preferences of each metal ion. Furthermore, its rigidity should help to restrict vibrational motion of ligands. Lacunary ligands of W POMs assure isolation of the metal ion from centers presenting nuclear spin $I \neq 0$. It is likely that all this favorable features will motivate the development of new transition metal-POM SMMs.

Acknowledgments

Authors acknowledge Proyectos Basales and Vicerrectoría de Investigación, Desarrollo e Innovación of Universidad de Santiago de Chile (USACH). D.A. thanks CONICYT + PAI "Concurso nacional de apoyo al retorno de investigadores/as desde el extranjero, convocatoria 2014 82140014". E.R. thanks Generalitat de Catalunya for an ICREA Academia grant. We thank CSUC (Consorci de Serveis Universitaris de Catalunya) for computational resources. Powered@NLHPC: This research was partially supported by the supercomputing infrastructure of the NLHPC (ECM-02). DV-Y is a member of CEDENNA Center (FB0807). D.A. thanks Professor M. Atanasov from Max-Planck Institute for Chemical Energy Conversion for routines to perform AILF analysis.

Supporting Information available: Cartesian coordinates of calculated models, a sample input file and additional results indicated in the text. This material is available free of charge via the Internet at http://pubs.acs.org.

References

(1) Ishikawa, N.; Sugita, M.; Ishikawa, T.; Koshihara, S. Y.; Kaizu, Y. *J. Am. Chem. Soc.* **2003**, *125* (29), 8694–8695.

(2) Powell, a K.; Heath, S. L.; Gatteschi, D.; Pardi, L.; Sessoli, R.; Spina, G.; Delgiallo, F.; Pieralli, F. *J. Am. Chem. Soc.* **1995**, *117* (9), 2491–2502.

(3) Zhong, Z. J.; Seino, H.; Mizobe, Y.; Hidai, M.; Fujishima, A.; Ohkoshi, S. I.; Hashimoto, K. *J. Am. Chem. Soc.* **2000**, *122* (12), 2952–2953.

(4) Murugesu, M.; Habrych, M.; Wernsdorfer, W.; Abboud, K. a; Christou, G. *J. Am. Chem. Soc.* **2004**, *126* (15), 4766–4767.

(5) Ako, A. M.; Hewitt, I. J.; Mereacre, V.; Clérac, R.; Wernsdorfer, W.; Anson, C. E.; Powell, A. K. *Angew. Chemie Int. Ed.* **2006**, *45* (30), 4926–4929.

(6) Kang, S.; Zheng, H.; Liu, T.; Hamachi, K.; Kanegawa, S.; Sugimoto, K.; Shiota, Y.; Hayami, S.; Mito, M.; Nakamura, T.; Nakano, M.; Baker, M. L.; Nojiri, H.; Yoshizawa, K.; Duan, C.; Sato, O. *Nat. Commun.* **2015**, *6*, 5955.

(7) Sessoli, R.; Gatteschi, D.; Caneschi, A.; Novak, M. A. *Nature* **1993**, *365*, 141–143.

(8) Milios, C. J.; Vinslava, A.; Wernsdorfer, W.; Moggach, S.; Parsons, S.; Perlepes, S. P.; Christou, G.; Brechin, E. K. *J. Am. Chem. Soc.* **2007**, *129* (10), 2754–2755.

(9) Aubin, S. M. J.; Wemple, M. W.; Adams, D. M.; Tsai, H. L.; Christou, G.; Hendrickson, D. N. *J. Am. Chem. Soc.* **1996**, *118* (33), 7746–7754.

(10) Waldmann, O. *Inorg. Chem.* **2007**, *46* (24), 10035–10037.

(11) Ruiz, E.; Cirera, J.; Cano, J.; Alvarez, S.; Loose, C.; Kortus, J. *Chem. Commun.* **2008**, *2* (1), 52–54.

(12) Neese, F.; Pantazis, D. A. *Faraday Discuss.* **2011**, *148*, 229–238.

(13) Frost, J. M.; Harriman, K. L. M.; Murugesu, M. *Chem. Sci.* **2016**, *7* (4), 2470–2491.

(14) Woodruff, D. N.; Winpenny, R. E. P.; Layfield, R. a. *Chem. Rev.* **2013**, *113* (7), 5110–5148.

(15) Gómez-Coca, S.; Aravena, D.; Morales, R.; Ruiz, E. *Coord. Chem. Rev.* **2015**, *289–290*, 379–392.

(16) Craig, G. A.; Murrie, M. *Chem. Soc. Rev.* **2015**, *44* (8), 2135–2147.

(17) Ishikawa, N.; Sugita, M.; Wernsdorfer, W. *J. Am. Chem. Soc.* **2005**, *127* (11), 3650–3651.

(18) Ganivet, C. R.; Ballesteros, B.; de la Torre, G.; Clemente-Juan, J. M.; Coronado, E.; Torres, T. *Chem. - A Eur. J.* **2013**, *19* (4), 1457–1465.

(19) Jeletic, M.; Lin, P. H.; Le Roy, J. J.; Korobkov, I.; Gorelsky, S. I.; Murugesu, M. *J. Am. Chem. Soc.* **2011**, *133* (48), 19286–19289.

(20) Zadrozny, J. M.; Xiao, D. J.; Atanasov, M.; Long, G. J.; Grandjean, F.; Neese, F.; Long, J. R. *Nat Chem* **2013**, *5* (7), 577–581.

(21) Poulten, R. C.; Page, M. J.; Algarra, A. G.; Le Roy, J. J.; López, I.; Carter, E.; Llobet, A.; Macgregor, S. a; Mahon, M. F.; Murphy, D. M.; Murugesu, M.; Whittlesey, M. K. *J. Am. Chem. Soc.* **2013**, *135* (37), 13640–13643.

(22) Westerström, R.; Dreiser, J.; Piamonteze, C.; Muntwiler, M.; Weyeneth, S.; Brune, H.; Rusponi, S.; Nolting, F.; Popov, A.; Yang, S.; Dunsch, L.; Greber, T. *J. Am. Chem. Soc.* **2012**, *134* (24), 9840–9843.

(23) AlDamen, M. A.; Clemente-Juan, J. M.; Coronado, E.; Martí-Gastaldo, C.; Gaita-Ariño, A. *J. Am. Chem. Soc.* **2008**, *130* (28), 8874–8875.

(24) AlDamen, M. a.; Cardona-Serra, S.; Clemente-Juan, J. M.; Coronado, E.; Gaita-Ariño, A.; Martí-Gastaldo, C.; Luis, F.; Montero, O. *Inorg. Chem.* **2009**, *48* (8), 3467–3479.

(25) Baldoví, J. J.; Clemente-Juan, J. M.; Coronado, E.; Duan, Y.; Gaita-Ariño, A.; Giménez-Saiz, C. *Inorg. Chem.* **2014**, *53* (18), 9976–9980.

(26) Baldoví, J. J.; Clemente-Juan, J. M.; Coronado, E.; Gaita-Ariño, A. *Inorg. Chem.* **2014**, *53* (20), 11323–11327.

(27) Sato, R.; Suzuki, K.; Minato, T.; Shinoe, M.; Yamaguchi, K.; Mizuno, N. *Chem. Commun.* **2015**, *51*, 4081–4084.

(28) Neese, F. *Wiley Interdiscip. Rev. Comput. Mol. Sci.* **2012**, *2*, 73–78.

(29) An ab initio, DFT and semiempirical SCF-MO package-Version 3.0 Design and Scientific Directorship: F. Neese; Technical Directorship: F. Wennmohs, Max-Planck-Institute for Chemical Energy Conversion Stiftstr. 34-36, 45470 Mülheim a. d. Ruhr, Germany, tccec@mpi-mail.mpg.de. With contributions from: U. Becker, D. Bykov, D. Ganyushin, A. Hansen, R. Izsak, D.G. Liakos, C.Kollmar, S. Kossmann, D.A. Pantazis, T. Petrenko, C. Reimann, C. Riplinger, M.Roemelt, B. Sandhöfer, I. Schapiro, K. Sivalingam, B. Wezisla, and contributions from our collaborators: M. Kallay, S. Grimme, E. Valeev, G. Chan.

(30) Roos, B. O.; Malmqvist, P.-A. *Phys. Chem. Chem. Phys.* **2004**, *6*, 2919–2927.

(31) Malmqvist, P.-Å.; Roos, B. O. *Chem. Phys. Lett.* **1989**, *155*, 189–194.

(32) Angeli, C.; Cimiraglia, R.; Evangelisti, S.; Leininger, T.; Malrieu, J.-P. *J. Chem. Phys.* **2001**, *114*, 10252.

(33) Angeli, C.; Cimiraglia, R.; Malrieu, J.-P. *Chem. Phys. Lett.* **2001**, *350*, 297–305.

(34) Rösch, N.; Krüger, S.; Mayer, M.; Nasluzov, V. A. In *Recent Developments and Applications of Modern Density Functional Theory*; Seminario, J., Ed.; Elsevier, 1996; Vol. 4, pp 497–566.

(35) Nakajima, T.; Hirao, K. *Chem. Rev.* **2012**, *112*, 385–402.

(36) Reiher, M. *Wiley Interdiscip. Rev. Comput. Mol. Sci.* **2012**, *2*, 139–149.

(37) Reiher, M. *Theor. Chem. Acc.* **2006**, *116*, 241–252.

(38) Pantazis, D. A.; Chen, X. Y.; Landis, C. R.; Neese, F. *J. Chem. Theory Comput.* **2008**, *4* (6), 908–919.

(39) Weigend, F.; Ahlrichs, R. *Phys. Chem. Chem. Phys.* **2005**, *7*, 3297–3305.

(40) Schafer, A.; Horn, H.; Ahlrichs, R. *J. Chem. Phys.* **1992**, *97* (4), 2571–2577.

(41) Sinnecker, S.; Rajendran, A.; Klamt, A.; Diedenhofen, M.; Neese, F. *J. Phys. Chem. A* **2006**, *110* (6), 2235–2245.

(42) Atanasov, M.; Ganyushin, D.; Sivalingam, K.; Neese, F. In *Molecular Electronic Structures of Transition Metal Complexes II*; Mingos, D. M. P., Day, P., Dahl, J. P., Eds.; Structure and Bonding; Springer Berlin Heidelberg, 2012; pp 149–220.

(43) Atanasov, M.; Aravena, D.; Suturina, E.; Bill, E.; Maganas, D.; Neese, F. *Coord. Chem. Rev.* **2015**, *289-290*, 177–214.

(44) Schweinfurth, D.; Sommer, M. G.; Atanasov, M.; Demeshko, S.; Hohloch, S.; Meyer, F.; Neese, F.; Sarkar, B. *J. Am. Chem. Soc.* **2015**, *137*, 1993–2005.

(45) Yamatera, H. *Bull. Chem. Soc. Jpn.* **1958**, *31* (1), 95–108.

(46) Schäffer, C. E.; Jørgensen, C. K. *Mol. Phys.* **1965**, *9* (5), 401–412.

(47) Alvarez, S.; Alemany, P.; Casanova, D.; Cirera, J.; Llunell, M.; Avnir, D. *Coord. Chem. Rev.* **2005**, *249*, 1693–1708.

(48) Llunell, M.; Casanova, D.; Cirera, J.; Alemany, P.; Alvarez, S. 2010.

(49) Gomez-Coca, S.; Cremades, E.; Aliaga-Alcalde, N.; Ruiz, E. *J. Am. Chem. Soc.* **2013**, *135* (18), 7010.

(50) Ungur, L.; Chibotaru, L. F. In *Lanthanides and Actinides in Molecular Magnetism*; Layfield, R., Murugesu, M., Eds.; Wiley-VCH Verlag GmbH & Co. KGaA, 2015; pp

153–184.

(51) Ungur, L.; Thewissen, M.; Costes, J.-P.; Wernsdorfer, W.; Chibotaru, L. F. *Inorg. Chem.* **2013**, *52*, 6328–6337.

(52) Pugh, T.; Tuna, F.; Ungur, L.; Collison, D.; McInnes, E. J. L.; Chibotaru, L. F.; Layfield, R. a. *Nat. Commun.* **2015**, *6*, 7492.

(53) Neese, F.; Petrenko, T.; Ganyushin, D.; Olbrich, G. *Coord. Chem. Rev.* **2007**, *251*, 288–327.

(54) Radoń, M.; Gąssowska, K.; Szklarzewicz, J.; Broclawik, E. *J. Chem. Theory Comput.* **2016**, DOI: 10.1021/acs.jctc.5b01234.

(55) Stavretis, S. E.; Atanasov, M.; Podlesnyak, A. A.; Hunter, S. C.; Neese, F.; Xue, Z.-L. *Inorg. Chem.* **2015**, *54* (20), 9790–9801.

(56) Gómez-Coca, S.; Urtizberea, A.; Cremades, E.; Alonso, P. J.; Camón, A.; Ruiz, E.; Luis, F. *Nat. Commun.* **2014**, *5* (123), 5:4300.

(57) Tanabe, Y.; Sugano, S. *J. Phys. Soc. Japan* **1956**, *11* (8), 864–877.

(58) Tanabe, Y.; Sugano, S. *J. Phys. Soc. Japan* **1954**, *9* (5), 766–779.

(59) Jørgensen, C. K. *Oxidation Numbers and Oxidation States*; Springer-Verlag: New York, 1969.

(60) Sugar, J.; Corliss, C. *Atomic energy levels of the iron-period elements: potassium through nickel*; American Chemical Society and the American Institute of Physics for the National Bureau of Standards: New York, 1985; Vol. 14.

For Table of Contents Only

Single Molecule Magnet Properties of Transition Metal Ions encapsulated in Lacunary Polyoxometalates: a Theoretical Study

Daniel Aravena, Diego Venegas-Yazigi, Eliseo Ruiz

TOC Synopsis: Single molecule magnet properties of transition metals coordinated to lacunary polyoxometalates are analyzed using state of the art *ab initio* methods. Three isostructural complexes (Co^{II}, Mn^{III} and Fe^{III}) are studied. The electronic structure of the Fe^{III} compound is studied in detail as a rare example of a high spin d^5 center exhibiting field-induced single molecule magnet behavior.

TOC graphic